Chapter 1

Prediction of print success for concrete 3D printing

Pieter Collins[1], Simcha van Helvoort[2], Giorgi Khimshiasvili[3], Antonio Marsella[1], Jaap Molenaar[4], Lense Swaenen[5]

[1]Maastricht University, The Netherlands
[2]Fontys Hogeschool, The Netherlands
[3]Ilia State University, Georgia
[4]Wageningen University, The Netherlands
[5]Sioux Lime, The Netherlands

Abstract:
Bruil beton & mix is specialized in the production of concrete for all kinds of applications. In the past years, Bruil has developed a new, exciting technique that has revolutionized this sector: production of prefab elements using concrete 3D printing. This development offers architects a completely new scala of design possibilities in form, colour, and structure. 3D printing starts with a digital 3d model of the object. From this 3D model a print path is created, based on the required layer width and height. Code based on the created print path, will steer the movements of the concrete printer. Using these movements to deposit concrete at the right locations, the 3D printing process thus results in a printed concrete object. There are several difficulties with 3d printing of concrete. One of them is that concrete is a material of which the properties change during the drying process. Furthermore, these properties quite strongly depend on external conditions. Therefore, in practice there are many variables that influence the printing result and thus determine whether a print will be successful: material properties, environmental conditions, rheology, the shape of the growing object, print speed etc. Second, not all structures dreamt up on the drawing table can be easily produced with 3D printing. During the printing process the emerging structure could start to bend, collapse and/or deform, depending on geometry and material properties. So, the drying process and the printing process should be fine-tuned, to allow for efficient, fast, and reliable production of 3D objects.
In this report we first present some checks on printability that are easily implemented in practice. Then, we dealt with the question whether the stress profile during the printing process fulfils the condition that the developing structure does not collapse under its own weight. To answer that question, we study a variety of different approaches to calculate the stress profile. These approaches range from several approximating analytical methods to numerical simulations. The conclusion is that for simple geometries, such as a tilted wall, analytical, explicit formulae can be used to check stress conditions, but that for general geometries a numerical approach, based on, e.g., a finite element method, is indispensable.

KEYWORDS: *3D-printing, concrete, stress conditions, perturbation method, finite element method*

1.1 Introduction

3D printing of concrete is a recent breakthrough in the construction world. In the traditional approach of building with concrete, the fresh material is poured in a form work, that has been designed according to the required final shape. After a drying period in which the concrete hardens, the form work is taken away and a solid structure results. In contrast, 3D printing is a completely different concept. The fresh material is extruded via a nozzle in a continuous way. The extruded material forms a flexible thread of concrete that is laid upon or against earlier layers. By steering the spray head along a well chosen, predefined path, all kinds of shapes can be formed. The 3D printing technique has revolutionized this sector, since it allows for many new applications of concrete. It offers architects a completely new scala of design possibilities in form, colour, and structure. See for example figure section 1.1.

Concrete companies like Bruil apply 3D printing already in practice, but are faced with several challenges. One of the possible problems that may arise stems from the fact that concrete changes its properties while hardening. For example, a layer that is being extruded has other properties than the layer on top of which it is deposited. If the differences are too large, it may happen that the neighboring layers do not neatly stick to each other, with as result that the structure of the final object is not completely uniform. Another complication may be that the bottom layers are not hardening fast enough to bear the layers above them. In that case the bottom layers will start to flow side wards and the whole construction will collapse. Still another source of problems may be that, while under construction, the centre of gravity of the construction shifts every time a new layer is added. This may cause the object to topple.

All these aspects force the constructor to carefully design the printing process: the printing process should be fine-tuned such that it allows for efficient, fast, and still reliable production. In this report we deal with a number of sensitive aspects of the printing process. In section 2 we discuss the minimum requirements to be satisfied while printing. The speed of the printing head when hovering over the object under construction and the rate of deposition should be chosen not too low on the one hand, since otherwise the concrete is already hardening too much in the printing head, but on the other hand not too high since then the preceding layers are not yet hardened enough. In building up a tilted object layer by layer, its centre of mass should remain positioned such that the object will not topple. In section 3 we pay attention to structural analysis checks: does the hardening process remain under control so that the construction does not collapse under its own weight. We analyse the stress equations in several ways. First, they are implemented in a Finite Element Package and evaluated on the computer. The

advantage of this approach is that this allows the analysis of all kinds of shapes. On the other hand, computer simulations may be costly and do not always converge. Second, in a complementary endeavour, we follow a number of analytical approaches to solve the stress model equations for special shapes in an approximating way. The results give rise to new insights, that would not have been obtained if we had stuck to computer simulations only. This is especially advantageous for the printing daily practice, since in the procedure of designing the printing process one is often particularly interested in rules of thumb.

We conclude this report with formulating a set of recommendations. These are partly very practically oriented, but we also advocate to involve computer simulations of the stress and strain profiles of the material into the preparation of the printing process, since only such an analysis can yield definite answers if non standard shapes have to be printed.

Figure 1.1: Example of 3D printed concrete object (copyright Bruil).

1.2 Direct printability checks

In this section we formulate some printability checks that can easily be performed once the path of the printing head and the concrete flow rates have been chosen for a specific geometry.

1.2.1 Flows and rates

Fundamental printing path parameters, to be set by the user:

- ρ: Flow rate,
- h_l: Layer height,
- w_l: Layer width,
- l_l: Layer path length.

In addition, we have

- l_l: Layer path length,

which follows from the geometry under consideration.
We consider 4 checks:

1. The flow rate should be such high that the concrete does not dry while still in the hose. This can be simply expressed as

$$\rho \geq \rho_{\min}. \tag{1.1}$$

2. The hose has a maximum flow capacity. This can be simply expressed as

$$\rho \leq \rho_{\max}. \tag{1.2}$$

3. The concrete should form a homogeneous mass and should not exhibit stratification (layering) which compromises structural integrity. The most natural expression of this constraint is that the time between layers should be below a certain value $t_{\max}$, typically 2 minutes. During the printing, it is not possible to wait between layers, as this produces geometrical artifacts not acceptable for design purposes. The time per layer is therefore

$$\text{time per layer} = \frac{\text{volume per layer}}{\text{flow rate}}. \tag{1.3}$$

This leads to the condition

$$\frac{h_l w_l l_l}{\rho} \leq t_{\max}. \tag{1.4}$$

4. The concrete should be solid enough to support the layers on top of it. This questions can be considered very generally as a structural analysis problem, and is treated as such in section 1.3. However, for simple geometries like a straight column, a check can be formulated in terms of the 4 fundamental user settings used above; see Perrot [2]. He proposes as criterion that the height rate at which the structure grows, should be below a certain value H, typically 1.5 meters per hour. The height rate can be related to the layer height and time per layer. This condition can be written as:
$$\frac{\rho}{w_l l_l} \leq H, \tag{1.5}$$
but we emphasize that this criterion will certainly not hold in general.

1.2.2 Centre of mass

Since the printed structure is not attached to the floor in any way, the centre of mass must lie above the convex hull of the base. The centre of mass can be computed cheaply, for every desired time (e.g., per layer) as shown below.

Assume a possibly time-dependent flow rate $\rho(t)$, with the concrete being deposited at a point $(x(t), y(t), z(t))$. Then the total volume $V(t)$ is given by

$$V(t) = \int_0^t \rho(\tau) d\tau \,, \tag{1.6}$$

and the x- and y-coordinates of the centre of mass are

$$\bar{x}(t) = \frac{1}{V(t)} \int_0^t \rho(\tau) x(\tau) d\tau \,, \quad \bar{y}(t) = \frac{1}{V(t)} \int_0^t \rho(\tau) y(\tau) d\tau \,. \tag{1.7}$$

For a small time increment δt,

$$V(t + \delta t) \approx V(t) + \rho(t)\delta t$$

and

$$\bar{x}(t + \delta t) = \frac{1}{V(t + \delta t)} \int_0^{t+\delta t} \rho(\tau) x(\tau) d\tau \quad \approx \frac{1}{V(t) + \rho(t)\delta t} \big(V(t)\bar{x}(t) + \rho(t)x(t)\delta t \big).$$

Taking measuring time points $t_0, t_1, \ldots$, and writing $\delta t_n = t_{n+1} - t_n$ we may thus simply follow the centre of mass coordinates in time by evaluating the update formulae

$$\begin{gathered} V(t_{n+1}) \approx V(t_n) + \rho(t_n)\delta t_n \,, \\ \bar{x}(t_{n+1}) \approx \frac{V(t_n)\bar{x}(t_n) + \rho(t_n)x(t_n)\delta t_n}{V(t_{n+1})} \,, \quad \bar{y}(t_{n+1}) \approx \frac{V(t_n)\bar{y}(t_n) + \rho(t_n)y(t_n)\delta t_n}{V(t_{n+1})} \,. \end{gathered} \tag{1.8}$$

It would also be possible to obtain more accurate estimates using higher-order integration methods such as Simpson's rule, but taking δt small is probably enough to obtain good accuracy.

As mentioned in the beginning of this section, the center-of-mass should be in the convex hull of the support not to topple. However, when on the boundary of the convex hull, one can expect all of the weight of the structure to be concentrated on a tiny portion of the support, which makes a structural failure more likely. One could shrink the support a certain amount to improve stability. A relationship between the height/mass of the structure and how much to shrink the support can probably be derived.

The center-of-mass makes for a nice bridge to more fundamental structural analysis, as center-of-mass is already a matter of balances of forces. We finally remark that one could use the lateral force required to topple the structure and calculated in a stress analysis, as another way to get some margin on the center-of-mass check.

1.3 Stress checks

In this section we discuss the printability restrictions that follow from the stresses in the drying concrete. To calculate the stresses at equilibrium we have to solve the so-called stress equations for the stress tensor $\boldsymbol{\sigma}$ with components:

$$\boldsymbol{\sigma} = \begin{pmatrix} \sigma_{xx} & \sigma_{xy} & \sigma_{xz} \\ \sigma_{xy} & \sigma_{yy} & \sigma_{yz} \\ \sigma_{xz} & \sigma_{yz} & \sigma_{zz} \end{pmatrix} . \tag{1.9}$$

At equilibrium, the stress satisfies

$$\boldsymbol{\nabla} \cdot \boldsymbol{\sigma} = -\boldsymbol{f} \,, \tag{1.10}$$

where $\boldsymbol{f}$ is the force density in the body. Under gravity, $\boldsymbol{f} = \rho\, g\, \boldsymbol{e}_z$. The acceleration of gravity g has the value $g \approx 9.81 m\, s^{-2}$. The boundary conditions for a free surface with normal $\boldsymbol{n}$ are $\boldsymbol{n} \cdot \boldsymbol{\sigma} = \boldsymbol{0}$.
The units of stress are $N m^{-2} \equiv kg\, m^{-1} s^{-2}$.

The most important insight to be taken into account is that drying concrete has a yield stress that depends on the drying history of the material and thus on time. Note that in a pile of several concrete layers, each of which deposited at a different time, the

yield stress varies per layer and in time. As long as the local stress remains below the local yield stress, the concrete will stay at rest, not flow and thus not deform. When one concrete layer has been deposited, the material will have a certain stress distribution. In general the stress will be highest at the bottom and lowest (maybe vanishing) at the top of the layer. In the next round of printing a new layer will be deposited on the first one. This will change the stress distribution in the first layer. At that moment the stress distributions in the first and the new layer have to be calculated and it should be checked whether the maximum stress remains below the yield stress everywhere. If a third layer is deposited, the stress check has to be repeated but now for three layers. And so on for an arbitrary number of layers. If at some moment in time at some point in the material the stress condition is not fulfilled, the printing procedure will not lead to a robust build up of the desired geometry. These stress checks can be applied before printing starts, through simulation of the stress distributions in space and time on the computer, together with keeping track of the time and position dependent yield stress distribution. In the subsections below we show how the required stress calculations can be done for a variety of geometries. We first show results from numerical (computer) simulations. Thereafter we also present results from analytical approaches.

1.3.1 Numerical approach

The holy grail for this problem would be a simulation that takes the 3D printing model as input and a True value as output if the structure is printable and a False value as output if the structure is not printable. This section is proposing a way to simulate the printing part with the 3D printing model as input.
For large scale production, with structures that are not the same, every structure needs to undergo these checks. Importantly, a calculation time longer than ten minutes is not desirable.
For the FEM simulations, we used the MATLAB PDE toolbox.

Modeling approach

When concrete is stiffening, a change in the elasticity modulus is expected. The concrete comes out of the nozzle already stiffened up, but still wet enough to merge with the neighbouring layers as described in section 1.2.1.

We do not know what the elasticity modulus is over time, so a couple of checks have been made. For three types of structures the simulations have been run with different Young's Modulus. As seen in fig. 1.2, the Young's modulus has no effect for these struc-

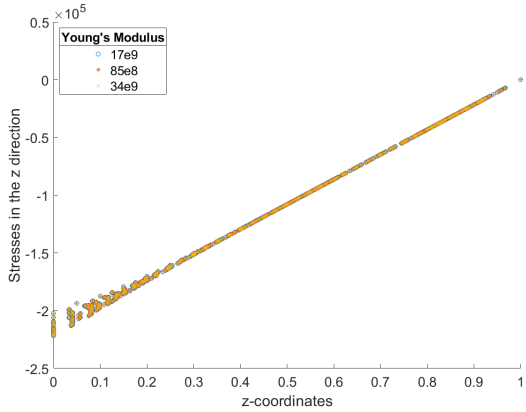

(a) Z-Stresses for a straight beam.

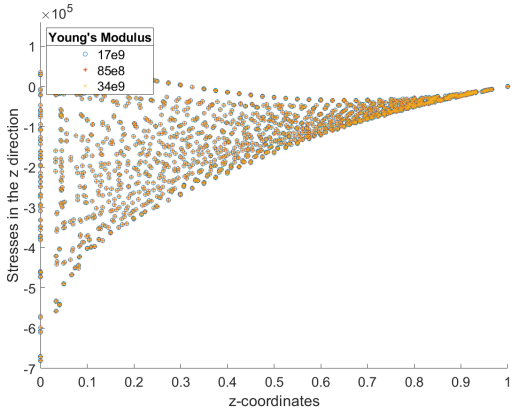

(b) Z-Stresses for a tilted beam.

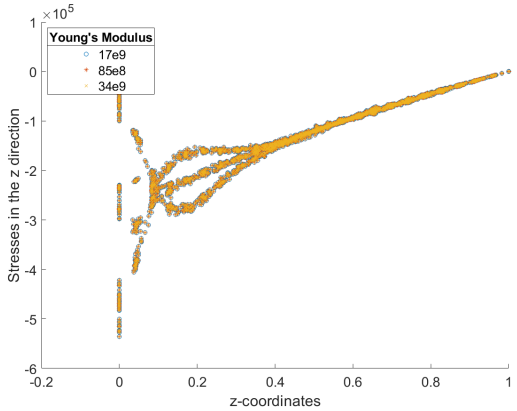

(c) Z-Stresses for a hollow cone.

Figure 1.2: Comparison of the Z-stresses for different Young's Moduli for various structures.

tures. Whether the Young's modulus is down or up a factor of two, the results are the same.

This makes the problem time invariant and only height variant. To simulate layering, we varied the z-coordinates before meshing. This required making a new mesh every iteration and this is very computationally expensive since calculation time per iterations will increase exponentially with mesh size. A possible solution will be proposed in section 1.4, but for the present simulations we didn't apply this idea yet.

The boundary condition applied at the bottom of the object deserves special attention. The concrete object does not stick to the table. A realistic boundary condition for the contact between the table and the concrete would be hard contact, which allows pushing (positive normal stress) but not pulling (negative normal stress). Such a boundary condition is very challenging computationally, as the problem is no longer linear.

Moreover, the MATLAB PDEtoolbox does not have this feature. More specialized FEM packages like ANSYS allow for such boundary conditions by modelling both the support and the contact. If such a boundary condition is used, toppling of a structure (like in the center-of-mass checks) can also be derived from the structural analysis. In the ANSYS best practices manual, this is referred to as 'lift-off'. When the center-of-mass is outside of its support, there is no feasible distribution of stresses that does not have a normal stress at the table/concrete interface.

Another aspect is the shear stress at the bottom. Since there is friction between table and object, few shear stress will not cause the object to shift. Much shear stress, however, will lead to a shifting object. It is not clear what the critical shear stress is for drying concrete, so we could not specify it. In our calculations we assumed the object to be rigidly fixed to the table:

$$u(x, y, 0) = 0\,, \tag{1.11}$$

where $u(x, y, z)$ is the displacement of the object. This boundary condition was easy to implement within the MATLAB PDE toolbox.

Numerical solution via the finite element method(FEM)

The results of the FEM simulation are given in fig. 1.3, where the final, steady state stress distributions are shown. The computational times are given in table 1.1. These results can be checked via comparison with results from analytical approaches in the subsections below.

Structure	Computing time
Straight Beam	31 seconds
Tilted Beam	32 seconds
Hollow Cone	No layering simulation has been done

Table 1.1: Computing time for different structures. The computing time is the time it took to simulate the layering using MATLAB.

1.3.2 Analytical approaches

As solving stresses from a full Finite Element model is computationally rather expensive, in this section we explore analytical approaches to approximate stresses throughout the

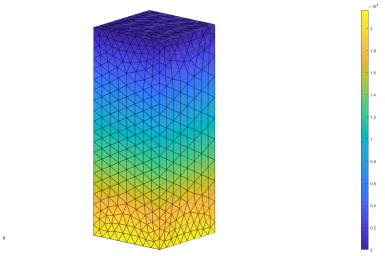

(a) FEM result for a straight beam.

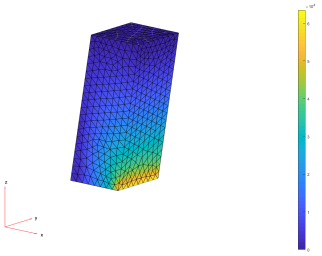

(b) FEM result for a tilted beam.

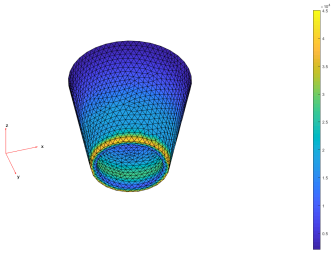

(c) FEM result for a hollow cone.

Figure 1.3: FEM steady state results for different kinds of structures.

geometry. Here, we derive analytical formulae for simple geometries. We emphasize that the present lines of thought are by far not yet complete, in view of the limited time that spanned the SWI 2019, but are meant to inspire further research. The results can be used to check the numerical results, but the insights may also be used to find rules of thumb for general geometries. We start with the simplest geometry, a straight wall, and incrementally move to more general geometries.

Buckling check

Three basic cases of straight wall structures were considered in a recent paper of A. Suiker [5]. We elaborate on the results of this paper concerned with elastic buckling by relating them to some basic results of catastrophe theory and outlining hypothetical analogous results on elastic buckling of wall structures of a slightly more general type described below. To this end we rely on the rigorous analysis of buckling of thin rods (Euler buckling) and thin elastic membranes given in the fundamental monograph of T.Poston and I.Stuart [6].

Consider the model of 3D printing of a rectangular wall used in the paper of A. Suiker. The wall is given by a rectangular, heterogeneous plate of length L, width b and thickness h subjected to in-plane forces acting in the mid-plane of the plate. It is assumed that

this wall is produced by a 3D printing process, with linear curing function, applied in the direction of length L (i.e., L should be considered as the height of wall) which is characterized by the following parameters:

- constant wall growth velocity in vertical direction $l^* = Q/(hv_hT_l)$,
- the initial bending stiffness $D = (Eh^3)/(12(1-\gamma^2))$,
- dimensionless parameter $\mu = \rho g(h/D)(l^*/\phi)$,

where Q is the material volume delivered by the nozzle per unit time, v_h is the horizontal velocity of the nozzle, T_l is the time needed for printing one layer, ρ is the volumetric mass density, $g = 9.81m/s^2$ is the gravitational acceleration, γ is the Poisson modulus of material considered, E is the initial stiffness modulus, ϕ is the curing speed of the linear curing process. More detailed descriptions of the above quantities are given in [5].

As was shown in [5], both elastic buckling and plastic collapse can happen in this process and a criterion of the possible failure mechanism can be expressed in terms of geometrical, material and printing process data. Using the aforementioned data one can algorithmically calculate dimensionless quantities L_c, L_p and Λ and formulate the following criteria:

- elastic buckling happens if $L_c/L_p < \Lambda$,
- plastic collapse happens if $L_c/L_p > \Lambda$.

Here $\Lambda = (h/D)^{1/3}|\sigma|(\rho g)^{-2/3}$, where σ is the yield strength of material. The explicit formulae and computational algorithms for L_c and L_p are given in Eqs. (75), (91), (92), (94) of [5] .

Our first observation is that these criteria agree with the classical results on buckling of thin rods and elastic membranes given in Chapter 13 of the monograph [6]. To this end notice that, for small values of thickness h, the plate (wall) under consideration can be approximated by an elastic rectangular membrane of length L and width b so that membrane can be considered as a limit as $h \to 0$. Analogously, if both h and b tend to zero in a commensurable way, then the limiting object can be identified with an elastic thin rod of length (height) L. Then it is easy to verify that the above criteria agree with the classical criterion of Euler buckling described in [6].

Our second observation is aimed at obtaining similar results for vertical walls over more complicated horizontal bases. To this end consider a vertical wall $W(X, L, h)$ of height L and thickness h obtained as a tube of radius $h/2$ around a vertical plate of height L over a circular arc X of length b and curvature K in the horizontal plane. Such an object gives a natural generalization of the rectangular wall discussed above.
For such a circular wall, repeating the analysis given in [5] is easy. It yields that the condition for plastic collapse remains the same as for the rectangular wall considered above. The situation with elastic collapse is more interesting. For some models of 3D printing process, there exists numerical evidence that the curvature influences the critical height for elastic buckling by making it bigger than in the flat case. We are unable to give a rigorous proof of this fact and to give a hypothetical formula for the increase of critical height in terms of the curvature K. Elaborating on the influence of curvature of wall profile is an interesting mathematical challenge and, moreover, may appear useful for analysis of mechanical performance of 3D printing processes for walls over more general planar profiles.

Analytical approach: tilted wall with linear vertical normal stress variation

We consider a tilted wall of width w, angle θ with the vertical, and total height h, and try to approximate the stresses at any intermediate height. We make the following two assumptions:

1. Only σ_{zz} is non-zero. All other stresses are zero.

2. σ_{zz} varies linearly across the width at a certain height: $\sigma_{zz}(x, z) = a(z)x + b(z)$

Note that both assumptions hold for the non-tilted wall. A rationale for the second approximation comes from the fact that the thickness of the printed wall will be small compared to the other dimensions (length and height of the wall). Inspiration was drawn from somehttps://www.overleaf.com/project/5c63d9969a586b5c02a038ad figures in [1].

To derive approximate values for the vertical normal stress throughout the tilted wall, we consider a cross-section at a certain height, as in figure 1.4. h is the height of the part of the wall above this cross-section. According to the assumptions, the vertical normal stress varies linearly. The entire profile across the cross-section is therefore described completely by the two variables f_L and f_R. We now require that the block of material above the intersection should be in static equilibrium: both the balance of forces and the balance of moments should be zero. This leads to two equations that are linear in f_L and f_R. This system with 2 unknowns and 2 equations can be easily solved for f_L and f_R.

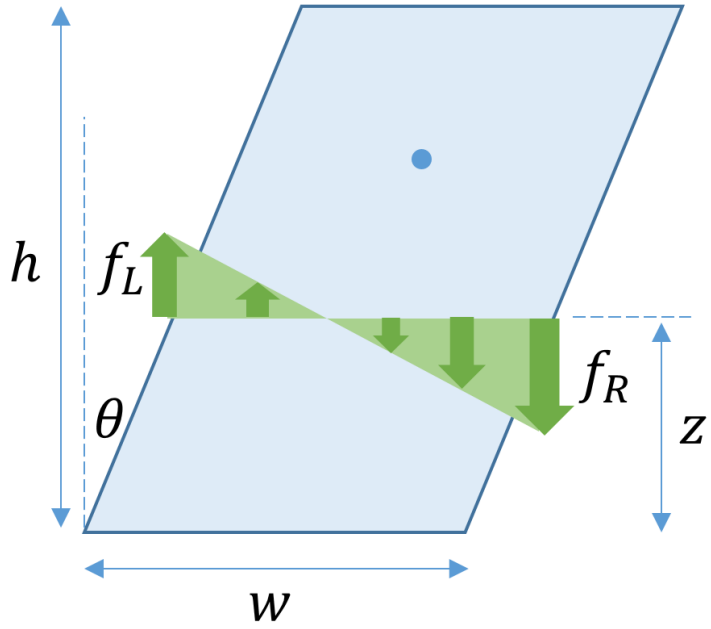

Figure 1.4: Approximate model diagram for the tilted wall.

The balance of forces reads

$$\int_{x_L}^{x_R} f(x)\,dx = mg\,, \tag{1.12}$$

with $x_R - x_L = w$. The forces at the interface need to counteract the gravity on the mass above the interface. Note that this mass is z-dependent: $m = \rho w(h - z)$. $f(x) \equiv \sigma_{zz}$ is the force at any point across the thickness:

$$f(x) = f_L + \frac{f_R - f_L}{w}(x - x_L). \tag{1.13}$$

The balance of forces can be formulated about any point. We choose x_L:

$$\int_{x_L}^{x_R} f(x)x\,dx = mg \cdot x_{CoM}, \tag{1.14}$$

with x_{CoM} the x-coordinate of the center-of-mass of the upper section. This leads to

$$x_{CoM} = \frac{w}{2} + (h - z) \cdot \tan(\theta). \tag{1.15}$$

Rewriting the integrals in equations (1.12) and (1.14) in terms of f_L and f_R yields the linear 2×2 system:

$$f_L + f_R = 2\frac{mg}{w} = 2\rho g(h - z), \tag{1.16}$$

$$f_L + 2f_R = 6\,\frac{mg \cdot x_{CoM}}{w^2}. \tag{1.17}$$

Solving for f_L and f_R yields:

$$f_L = \rho g(h-z)\left(1 - 3\frac{h-z}{w}\cdot\tan(\theta),\right) \tag{1.18}$$

$$f_R = \rho g(h-z)\left(1 + 3\frac{h-z}{w}\cdot\tan(\theta).\right) \tag{1.19}$$

These equations correctly reduce to the straight wall conditions for which $\theta = 0$. With $\theta > 0$, f_R now increases non-linearly with $h - z$, which has been also observed in the numerical FEM results. While f_R will be strictly positive for $\theta > 0$, we see how f_L can switch sign, indicating tensile stresses (inward/upward normal stress) in the material. Due to the tilt, one side of the wall experiences a downward 'pushing' force, whereas the other side experiences an upward 'pulling' force to compensate. Moreover, we observe that the non-linear term also has a dependency of $\frac{1}{w}$, which can also be understood intuitively: thin walls have a stronger push-pull action.

We compare the analytical results from this approximate model with the numerical results obtained earlier in figure 1.5. The stresses of the FEM mesh are plotted as a scatter plot. The stresses at the left and right faces are extreme (for a given height), so the modeled f_R and f_L should match the upper and lower envelopes. We observe the correct qualitative results, but quantitatively there is a definite mismatch. Through experimentation, we have observed that

$$f_{L,corr} = f_L - \rho g\frac{(h-z)^2}{w}\tan(\theta) = \rho g(h-z)\left(1 - 4\frac{h-z}{w}\cdot\tan(\theta)\right), \tag{1.20}$$

$$f_{R,corr} = f_R - \rho g\frac{(h-z)^2}{w}\tan(\theta) = \rho g(h-z)\left(1 + 2\frac{h-z}{w}\cdot\tan(\theta)\right). \tag{1.21}$$

match the numerical FEM results (for the upper section of the wall) almost perfectly. This correction can be seen as changing the multiplier of the non-linear terms in both equations; this correction is taken the same for both stresses. This means that in terms of the 2×2 balance of forces and moments equations, both the weight carried and the moments would need to be modified. It is not yet fully understood how and why this correction works. A possible explanation could be the model assumption that all stresses except σ_{zz} are 0. The FEM results show that this is not exactly true. If we compare the von Mises stress, which are given by

$$\sigma_{vm} = \frac{1}{\sqrt{2}}\sqrt{(\sigma_{xx}-\sigma_{yy})^2 + (\sigma_{yy}-\sigma_{zz})^2 + (\sigma_{zz}-\sigma_{xx})^2 + 6\sigma_{xy}^2 + 6\sigma_{yz}^2 + 6\sigma_{zx}^2}, \tag{1.22}$$

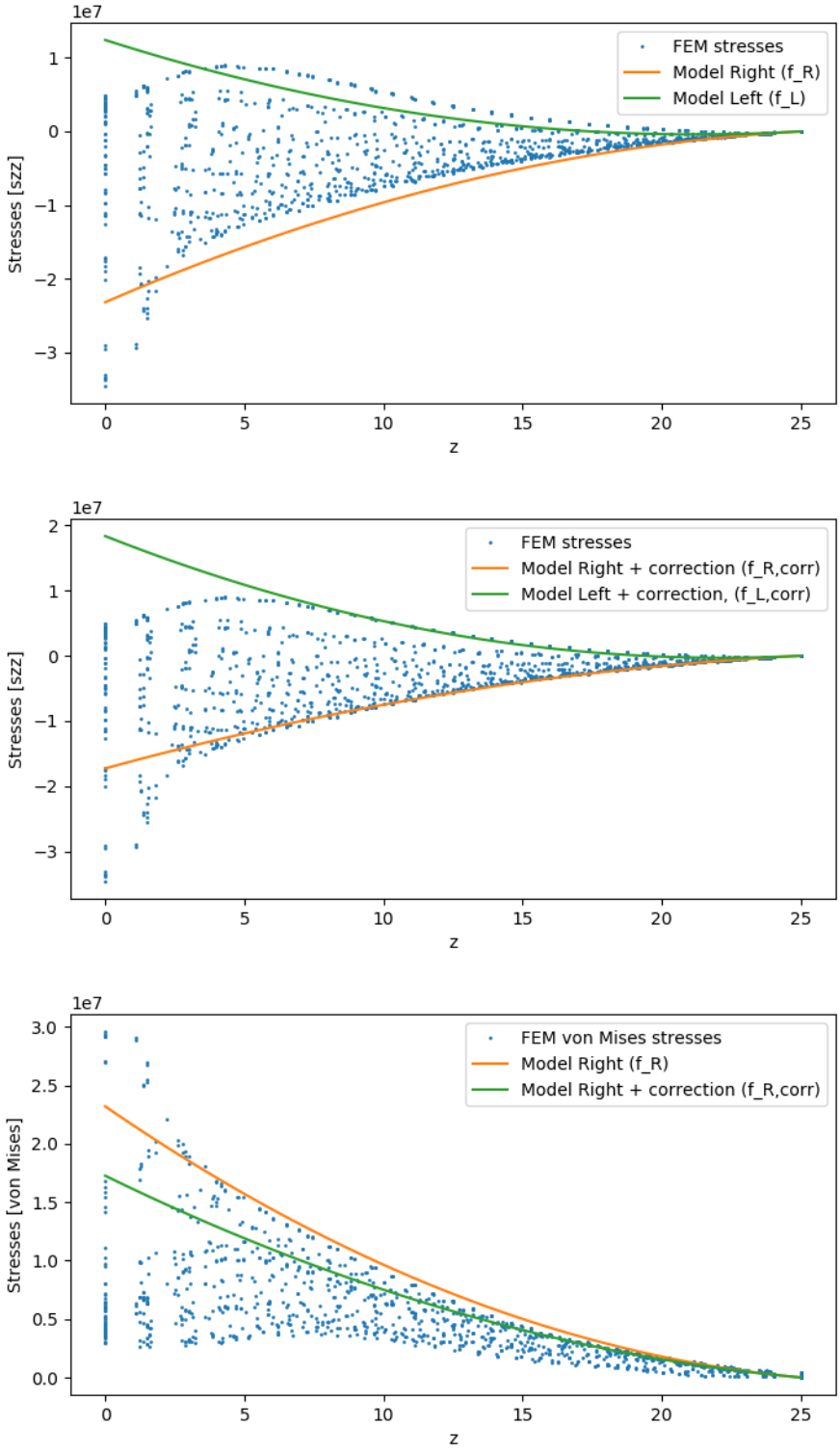

Figure 1.5: Comparison of FEM model with approximate model. Top: Comparing σ_{zz}. Middle: With correction added to the approximate model. Bottom: Comparing von Mises stresses.

then the original model already performs better.
Finally, we remark that the predicted quadratic behavior with $(h-z)^2$ is a good approximation in the upper section of the geometry, but near the bottom this description is clearly poor. Unfortunately, the bottom part is just the section we are most interested in, as stresses are highest and failure is most likely in that region. We observed earlier that the stresses at the bottom are quite sensitive to the boundary conditions chosen there. The present result again emphasizes that this boundary condition needs extra investigation.

Disregarding the accuracy of the approximation, this model has enabled us to derive local criteria on stability which look like $f_R(h-z,\theta,w) < \sigma_{max}$ which captures physics more realistically than the currently used $\theta < \theta_{max}$ criterion.

1.3.3 Analytical approach: separation of variables

We now consider an alternative approach to solve the stress equations for a number of geometries.

Vertical wall

Consider a vertical a wall of width w and height h. Omit the y-coordinate. Then the equilibrium equations become

$$\begin{aligned} \partial_x \sigma_{xx} + \partial_z \sigma_{xz} &= 0, \\ \partial_x \sigma_{xz} + \partial_z \sigma_{zz} &= -\rho g. \end{aligned} \tag{1.23}$$

The boundary conditions at the sides are

$$\sigma_{xx} = \sigma_{xz} = 0 \text{ when } x = 0 \text{ and } x = w. \tag{1.24}$$

The boundary conditions at the top are

$$\sigma_{xz} = \sigma_{zz} = 0 \text{ when } z = h. \tag{1.25}$$

An obvious solution of these equations is

$$\sigma_{xx} = \sigma_{xz} = 0; \quad \sigma_{zz}(x,z) = \rho g(h-z).$$

However, there are other solutions. Since the stress equations and boundary conditions are linear, any solution is the sum of a solution of the homogeneous equations (with r.h.s.

equal to zero) and a particular solution of the full, nonlinear equations. We show that the solutions of the homogeneous equations are not unique:

$$\begin{aligned} \partial_x \sigma^h_{xx} + \partial_z \sigma^h_{xz} &= 0, \\ \partial_x \sigma^h_{xz} + \partial_z \sigma^h_{zz} &= 0. \end{aligned} \tag{1.26}$$

The homogeneous equations have d a class of solutions of the following, separable form:

$$\sigma^h_{xx} = f_x(x) f''_z(z), \quad \sigma^h_{xz} = -f'_x(x) f'_z(z), \quad \sigma^h_{zz} = f''_x(x) f_z(z). \tag{1.27}$$

Suppose f_x satisfies $f_x(0) = f_x(w) = f'_x(0) = f'_x(w)$. Then any f_z satisfies the side boundary conditions. Similarly, if $f_z(h) = f'_z(h) = 0$, then any f_x satisfies the top boundary conditions. We can also consider homogeneous boundary conditions for the lower surface, $\sigma_{xz}(x,0) = \sigma_{zz}(x,0) = 0$.

We therefore have nontrivial solutions of the homogeneous equations, the simplest of which read as

$$f_x(x) = x^2(h-x)^2, \quad f_z(z) = z^2(h-z)^2,$$

yielding

$$\begin{aligned} \sigma^h_{xx} &= x^2(w-x)^2 \times 2(h^2 - 6hz + 6z^2), \\ \sigma^h_{xz} &= -2x(w-x)(w-2x) \times 2z(h-z)(h-2z), \\ \sigma^h_{zz} &= 2(w^2 - 6wx + 6x^2) \times z^2(h-z)^2, \end{aligned}$$

and

$$\sigma_{zz}(x,z) = 2(w^2 - 6wx + 6x^2) \times z^2(h-z)^2 + \rho g(h-z).$$

We can even set the horizontal stress at the bottom surface to zeros, $\sigma_{xx}(x,0) = 0$, requiring $f''_z(0) = 0$, and take $f_z(z) = z^3(h-z)^2$. This makes clear that there is an infinite-dimensional space of solutions to the homogeneous equations.

Remark 1.1. This shows that the equilibrium equations are underdetermined; in principle we need information about the stress-strain relationship to obtain a unique solution for the stress tensor. This likely means that to solve for the stresses, we in principle need to consider the dynamic processes involved as the concrete flows and sets while forming the object. In the following we take the simplest solution of the stress equations as the preferred one.

Tilted wall

In section 1.3.3 we sketch a vertical cross section of a tilted wall, of width w, height h, and inclination angle θ to the vertical. Let $\alpha = \tan\theta$, and $\xi = x - \alpha z$. Omit the y-coordinate.

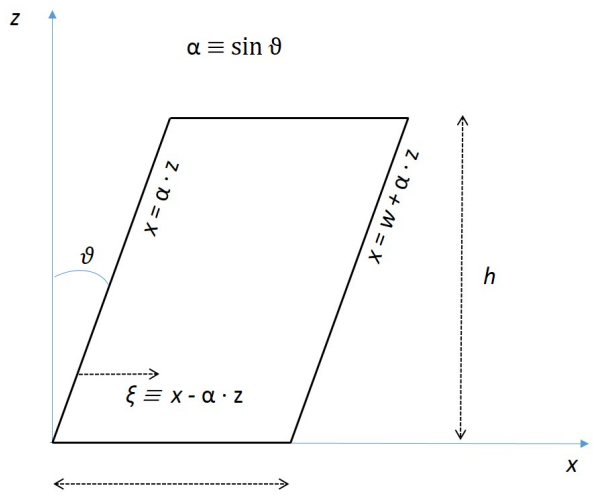

Figure 1.6: Vertical cross section along the x - axis of a tilted wall, of width w, height h, and angle of inclination θ. The wall is tilted in the (x, z) plane, but becomes vertical after application of the coordinate transformation $(x, z) \to (\xi, z)$.

Then the equilibrium equations become

$$\begin{aligned} \partial_x \sigma_{xx} + \partial_z \sigma_{xz} &= 0, \\ \partial_x \sigma_{xz} + \partial_z \sigma_{zz} &= -\rho g. \end{aligned} \tag{1.28}$$

The boundary conditions at the sides are

$$\left.\begin{aligned} \sigma_{xx} - \alpha \sigma_{xz} &= 0 \\ \sigma_{xz} - \alpha \sigma_{zz} &= 0 \end{aligned}\right\} \text{ when } x = \alpha z, \text{and} x = \alpha z + w. \tag{1.29}$$

The boundary conditions at the top are

$$\sigma_{xz} = \sigma_{zz} = 0 \text{ when } z = h. \tag{1.30}$$

For a frictionless supporting bottom surface the boundary condition would read as

$$\sigma_{xz} = 0 \text{ when } z = 0. \tag{1.31}$$

A simple particular solution σ^p of the full equations can be borrowed from the vertical wall, dealt with in the previous section:

$$\sigma^p_{xx} = \sigma^p_{xz} = 0; \quad \sigma^p_{zz}(x, z) = \rho g(h - z). \tag{1.32}$$

The full solution can be written as $\sigma = \sigma^h + \sigma^p$, where σ^p solves the homogeneous interior equations

$$\begin{aligned} \partial_x \sigma^h_{xx} + \partial_z \sigma^h_{xz} &= 0, \\ \partial_x \sigma^h_{xz} + \partial_z \sigma^h_{zz} &= 0. \end{aligned} \tag{1.33}$$

Then the boundary equations for σ^h become

$$\left.\begin{aligned}\sigma^h_{xx} - \alpha\sigma^h_{xz} &= 0\\ \sigma^h_{xz} - \alpha\sigma^h_{zz} &= \alpha\rho g(h-z)\end{aligned}\right\} \text{ when } x = \alpha z, \text{and} x = \alpha z + w \tag{1.34}$$

$$\sigma^h_{xz} = \sigma^h_{zz} = 0 \text{ when } z = h. \tag{1.35}$$

As above, we may try homogeneous solutions in separable form, and find a basis of solutions which satisfy:

$$\sigma^h_{xx} = f_x(x)f''_z(z), \quad \sigma^h_{xz} = -f'_x(x)f'_z(z), \quad \sigma^h_{zz} = f''_x(x)f_z(z). \tag{1.36}$$

We can also attempt to find homogeneous solutions of involving a function $f_\xi(\xi)$. The interior equations yield

$$\begin{aligned}\sigma^h_{xx} &= f_\xi(x-\alpha z)f''_z(z) - 2\alpha f'_\xi(x-\alpha z)f'_z(z) + \alpha^2 f''_\xi(x-\alpha z)f_z(z),\\ \sigma^h_{xz} &= -f'_\xi(x-\alpha z)f'_z(z) + \alpha f''_\xi(x-\alpha z)f_z(z), \quad \sigma^h_{zz} = f''_\xi(x-\alpha z)f_z(z).\end{aligned} \tag{1.37}$$

The side boundary conditions at $\xi_* = 0, w$ then become

$$\begin{aligned}f_\xi(\xi_*)f''_z(z) - 2\alpha f'_\xi(\xi_*)f'_z(z) + \alpha^2 f''_\xi(\xi_*)f_z(z) - \alpha\big(-f'_\xi(\xi_*)f'_z(z) + \alpha f''_\xi(\xi_*)f_z(z)\big) &= 0,\\ -f'_\xi(\xi_*)f'_z(z) + \alpha f''_\xi(\xi_*)f_z(z) - \alpha\big(f''_\xi(\xi_*)f_z(z)\big) &= \alpha\rho g(h-z).\end{aligned}$$

which simplifies to

$$\begin{aligned}f_\xi(0/w)f''_z(z) - \alpha f'_\xi(0/w)f'_z(z) &= 0\\ -f'_\xi(0/w)f'_z(z) &= \alpha\rho g(h-z).\end{aligned} \tag{1.38}$$

The top boundary conditions are then

$$-f'_\xi(\xi)f'_z(h) + \alpha f''_\xi(\xi)f_z(h) = 0, \quad f''_\xi(\xi)f_z(h) = 0. \tag{1.39}$$

Alternatively, we can formulate equations in terms of ξ and z. Taking $\tau_{\xi\xi}(\xi,t) = \sigma_{xx}(x-\alpha z, z) - \alpha\sigma_{xz}(x-\alpha z, z)$, $\tau_{\xi z}(\xi,t) = \sigma_{xz}(x-\alpha z, z) - \alpha\sigma_{zz}(x-\alpha z, z)$, $\tau_{zz}(\xi, z) = \sigma_{zz}(x-\alpha z, z)$ yields

$$\begin{aligned}\partial_\xi\tau_{\xi\xi} + \partial_z\tau_{\xi z} + \alpha\partial_z\tau_{zz} &= 0\\ \partial_\xi\tau_{\xi z} + \partial_z\tau_{zz} &= \alpha\rho g(h-z)\\ \left.\begin{aligned}\tau^h_{\xi\xi} &= 0\\ \tau^h_{\xi z} &= \alpha\rho g(h-z)\end{aligned}\right\} &\text{ when } \xi = 0, w.\end{aligned} \tag{1.40}$$

We then aim to find solutions of the homogeneous equations satisfying the boundary conditions

$$\left.\begin{aligned}\sigma^h_{xx} - \alpha\sigma^h_{xz} &= 0\\ \sigma^h_{xz} - \alpha\sigma^h_{zz} &= \alpha\phi(z)\end{aligned}\right\} \text{ when } x = \alpha z,\ x = \alpha z + w. \tag{1.41}$$

As in the case of the vertical wall, the equilibrium stress equations are underdetermined, and a full solution requires knowledge of the stress-strain relationship.

Decorative wall

Consider a decorative wall where the x-coordinate depends on the height: $\phi(z) \leq x \leq \phi(z) + w$. Let $\xi = x - \phi(z)$. We look for solutions of the homogeneous equations with

$$\sigma_{zz} = f''_\xi(x - \phi(z))f_z(z). \tag{1.42}$$

Then

$$\partial_x \sigma_{xz} - \phi'(z)f'''_\xi(x - \phi(z))f_z(z) + f''_\xi(x - \phi(z))f'_z(z) = 0,$$

so we can take

$$\sigma_{xz} = \phi'(z)f''_\xi(x - \phi(z))f_z(z) - f'_\xi(x - \phi(z))f'_z(z). \tag{1.43}$$

Similarly

$$\begin{aligned}\partial_x \sigma_{xx} - \phi'(z)^2 f'''_\xi(x - \phi(z))f_z(z) + \phi''(z)f''_\xi(x - \phi(z))f_z(z) \\ + 2\phi'(z)f''_\xi(x - \phi(z))f'(z) - f'_\xi(x - \phi(z))f''_z(z) = 0,\end{aligned}$$

so we can take

$$\begin{aligned}\sigma_{xx} = \phi'(z)^2 f''_\xi(x - \phi(z))f_z(z) - \phi''(z)f'_\xi(x - \phi(z))f_z(z) \\ - 2\phi'(z)f'_\xi(x - \phi(z))f'(z) + f_\xi(x - \phi(z))f''_z(z).\end{aligned} \tag{1.44}$$

Substituting $\xi = x - \phi(z)$ yields solutions of the form

$$\begin{aligned}\sigma_{zz} &= f''_\xi(\xi)f_z(z), \\ \sigma_{xz} &= \phi'(z)f''_\xi(\xi)f_z(z) - f'_\xi(\xi)f'_z(z), \\ \sigma_{xx} &= \phi'(z)^2 f''_\xi(\xi)f_z(z) - \phi''(z)f'_\xi(\xi)f_z(z) - 2\phi'(z)f'_\xi(\xi)f'(z) + f_\xi(\xi)f''_z(z).\end{aligned} \tag{1.45}$$

The inward normal to the boundary at the point $(\phi(z), z)$ is $(1, -\phi'(z))$, so the boundary conditions are

$$\begin{aligned}\sigma_{xx}(\phi(z), z) - \phi'(z)\sigma_{xz}(\phi(z), z) = 0, \\ \sigma_{xz}(\phi(z), z) - \phi'(z)\sigma_{zz}(\phi(z), z) = 0.\end{aligned} \tag{1.46}$$

with identical conditions holding at $(\phi(z) + w, z)$.

We look for separable solutions to the homogeneous equations with $f_\xi(\xi) = e^{i\kappa\xi} = \exp(i\kappa\xi)$. Further, we want κ to yield a wavelength dividing w, so $\kappa = \kappa_n = 2\pi n/w$. Then

$$\begin{aligned}f_\xi(\xi + w) &= \exp(i\kappa\xi + i\kappa w) = \exp(i\kappa\xi + 2\pi i n/w \times w) \\ &= \exp(i\kappa\xi + 2\pi i n) = \exp(i\kappa\xi) = f_\xi(\xi).\end{aligned}$$

Solving the homogeneous interior equations yields solutions in the following form:

$$\begin{aligned}
\sigma_{zz} &= -\kappa^2 f_\xi(\xi) f_z(z), \\
\sigma_{xz} &= -\kappa^2 f_\xi(\xi)\phi'(z) f_z(z) - i\kappa f_\xi(\xi) f_z'(z), \\
\sigma_{xx} &= -\kappa^2 f_\xi(\xi)\phi'(z)^2 f_z(z) - i\kappa f_\xi(\xi)\phi''(z) f_z(z) - 2i\kappa f_\xi(\xi)\phi'(z) f'(z) + f_\xi(\xi) f_z''(z).
\end{aligned} \tag{1.47}$$

At the left boundary value, $\xi = \phi(z)$. We aim to solve the boundary condition involving σ_{xx} exactly, yielding the differential equations

$$-\kappa^2\phi'(z)^2 f_z(z) - i\kappa\phi''(z) f_z(z) - 2i\kappa\phi'(z) f'(z) + f_z''(z) - \phi'(z)\big(-\kappa^2\phi'(z) f_z(z) - i\kappa f_z'(z)\big) = 0.$$

This simplifies to

$$-i\kappa\phi''(z) f_z(z) - i\kappa\phi'(z) f'(z) + f_z''(z) = 0.$$

The boundary term involving $\sigma_z z$ becomes

$$-\kappa^2 f_\xi(\xi)\phi'(z) f_z(z) - i\kappa f_\xi(\xi) f_z'(z) - \phi'(z)\big(-\kappa^2 f_\xi(\xi) f_z(z)\big),$$

which simplifies to

$$\sigma_{xz}(\phi(z), z) - \phi'(z)\,\sigma_{zz}(\phi(z), z) = -i\kappa\,\exp(i\kappa\phi(z))\,f_z'(z).$$

Summing over such terms gives

$$\sigma_{xz}(\phi(z), z) - \phi'(z)\,\sigma_{zz}(\phi(z), z) = \sum_{n=0}^{\infty} -ic_n\kappa_n\,\exp(i\kappa_n\phi(z))\,f_{z,n}'(z).$$

Conic wall

A natural next step in moving from simple to more complex geometries would be to generalize the tilted wall to conic walls, as visualized in figure 1.2. While a tilted wall is mainly parameterized by the height h, the width w and the slop θ, the conic wall has an additional radius r. One approach we would like to propose is that criteria such as the approximate ones derived for the tilted wall, like

$$f_{L,R}(h - z, \theta, w) < \sigma_{max} \tag{1.48}$$

should be generalized to criteria dependent on radius r, like

$$f_{L,R}(h - z, \theta, w, r) < \sigma_{max}. \tag{1.49}$$

One property one might expect/desire would be that

$$\lim_{r\to\infty} f_{L,R}(h - z, \theta, w, r) = f_{L,R}(h - z, \theta, w). \tag{1.50}$$

This expresses that the limit of the conic wall with a larger and larger radius is the straight wall. A second property one would like to require is that this limit is approached from below, as for a diverging cone, the curvature is expected to increase the stability of the structure. Mathematically one could formulate this as $f_{L,R}(h-z,\theta,w,r)$ being strictly increasing in r (though a rigorous formulation would require some more attention.

1.3.4 Analytical model: perturbation approach

Here, we show still another approach to obtain analytical approximations for the stresses in a tilted wall, sketched in section 1.3.3. The present method is based on expansion of the stress expressions in the parameter $\alpha = \tan(\theta)$, under the assumption $\alpha << 1$. In the (x,z) plane the stress equations read as

$$\begin{aligned} \partial_x \sigma_{xx} + \partial_z \sigma_{xz} &= 0, \\ \partial_x \sigma_{xz} + \partial_z \sigma_{zz} &= -\rho g. \end{aligned} \tag{1.51}$$

As already argued above, it is advantageous to apply the transformation $(x,z) \rightarrow (\xi,z)$ with ξ defined as $\xi = x - \alpha z$, since then the boundary conditions become simpler. After transformation the stress equations read as

$$\begin{aligned} \partial_\xi \sigma_{\xi\xi} - \alpha \partial_\xi \sigma_{\xi z} + \partial_z \sigma_{\xi z} &= 0, \\ \partial_\xi \sigma_{\xi z} - \alpha \partial_\xi \sigma_{zz} + \partial_z \sigma_{zz} &= -\rho g. \end{aligned} \tag{1.52}$$

The boundary conditions at the sides are

$$\left.\begin{aligned} \sigma_{\xi\xi} - \alpha \sigma_{\xi z} &= 0 \\ \sigma_{\xi z} - \alpha \sigma_{zz} &= 0 \end{aligned}\right\} \text{ when } \xi = 0 \,\text{and}\, \xi = w. \tag{1.53}$$

The boundary conditions at the top are

$$\sigma_{\xi z} = \sigma_{zz} = 0 \text{ when } z = h. \tag{1.54}$$

The boundary conditions at the bottom, where $z = 0$, should be such that the shear stress $\sigma_{\xi z}$ may not exceed the frictional force between object and table. However, this frictional force is proportional to the weight of the object with an unknown constant of proportionality, so we cannot specify this condition in detail.

For the vertical wall, i.e., when $\alpha = 0$, we have $\sigma_{\xi\xi} = \sigma_{\xi z} = 0$ and $\sigma_{zz} = \rho g(h-z)$. With respect to this zero-order solution, We write the first order expansions of the stresses in terms of α as

$$\begin{aligned} \sigma_{\xi,\xi} &= \alpha f_1 \xi, z, \\ \sigma_{\xi,z} &= \alpha f_2(\xi, z), \\ \sigma_{z,z} &= \rho g(h-z) + \alpha f_3(\xi, z). \end{aligned} \tag{1.55}$$

Substituting these expressions in the stress equations, we obtain

$$\begin{aligned} \partial_\xi f_1 + \partial_z f_2 &= 0, \\ \partial_\xi f_2 + \partial_z f_3 &= 0. \end{aligned} \tag{1.56}$$

with boundary conditions at the sides:

$$\left.\begin{aligned} f_1 &= 0 \\ f_2 &= \rho g(h-z) \end{aligned}\right\} \text{ when } \xi = 0, w. \tag{1.57}$$

and boundary conditions at the top:

$$f_2 = f_3 = 0, \text{ when } z = h. \tag{1.58}$$

Further progress requires specification of the stress-strain properties of concrete. But also without these details we may find a good approximation to the stress equations in the following way. We assume that f_2 is homogeneous in z and write $f_2 = \rho g(h-z) f_4(\xi)$ for some function $f_4(\xi)$. In view of the boundary conditions we must require $f_4(0) = f_4(w) = 1$. Substituting this in the stress equations we find

$$\partial_\xi f_1 = \rho g f_4(\xi), \tag{1.59}$$

with boundary conditions

$$f_1 = 0, \text{ when } \xi = 0, \text{and } \xi = w. \tag{1.60}$$

Its solution reads as

$$f_1 = f_1(\xi) = \rho g \int_0^\xi f_4(\xi') d\xi'. \tag{1.61}$$

This expression fits the boundary condition $f_1(\xi = 0) = 0$. To also fit the boundary condition $f_1(\xi = w) = 0$, we take for f_4 the simplest possible form, i.e., the parabola given by

$$f_4(\xi) = 6(\xi - (w/2)^2)/w^2 - 1/2. \tag{1.62}$$

and sketched in figure *section* 1.3.4. From the stress equations above we find that

$$\partial_z f_3 = \partial_\xi f_2 = -\rho g(h-z) f_4(\xi), \tag{1.63}$$

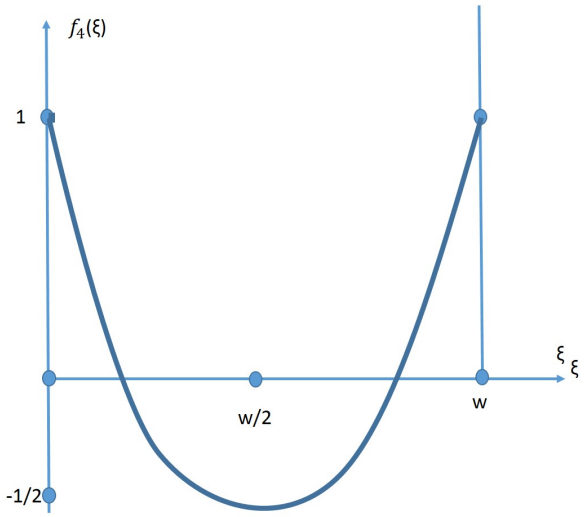

Figure 1.7: Sketch of the function $f_4(\xi) = 6(\xi - (w/2)^2)/w^2 - 1/2$.

with boundary condition

$$f_3(z = h) = 0. \tag{1.64}$$

Its solution reads as

$$f_3(\xi, z) = 6\rho g(z - h)^2(\xi - (w/2))/w^2. \tag{1.65}$$

Finally, we thus obtain for σ_{zz} the approximation

$$\sigma_{zz}(\xi, z) = \rho g(h - z) + \alpha f_3(\xi, z) = \rho g(h - z)[1 + 6\alpha(h - z)(\xi - (w/2))/w^2]. \tag{1.66}$$

This expression provides us with a useful approximation for the stress at the bottom of the tilted wall. Setting $z = 0$, we find that this stress is given by

$$\sigma_{zz}(\xi, 0) = \sigma_{zz}(x, 0) = \rho g h[1 + 6\alpha h(x - (w/2))/w^2]. \tag{1.67}$$

We observe that the extra stress due to the tilt of the wall varies linearly with the horizontal direction x. This was an assumption made in section 3.2.2. The present analysis confirms the correctness of this assumption for relatively small tilt of the wall. The maximum of the extra stress due to tilt is found in the right lower corner with coordinates $(w, 0)$. The vertical stress in that point is given by

$$\sigma_{zz}(w, 0) = \rho g h[1 + 3\alpha h/w]. \tag{1.68}$$

Since this is also the maximum stress in the whole wall, each stress check should focus at this value and make sure that this maximum stress does not exceed the yield stress in that corner point.

1.4 Recommendations

Based on the analysis presented above, we summarize the following recommendations:

- Flow rate checks
  - Concrete should not dry while in hose: Flow rate $\geq F_{min}$.
  - Maximum hose capacity: Flow rate $\leq F_{max}$.
- Stratification checks
  - Time per layer $<$ 2 L / min.
  - Time per layer = Volume per layer / flow rate.
  - Volume per layer = layer height $\cdot$ layer width $\cdot$ path length of layer.
- Center-of-mass check
  - Calculate in advance the position of the centre of mass, using the formulae in *section* 1.2.2 for all times of the printing process and check whether the object under construction runs the risk to topple.
- Stress Checks
  - Every round a new layer has been deposited the stress distribution in the object under construction changes. If locally the internal stress exceeds the local yield stress that part of the object will start to flow or collapse. So, the stress distribution has to be continuously calculated or estimated. With this information it should be checked whether the local stress is everywhere below the local yield stress. Note that the local yield stress depends on the local history thus on the time elapsed since that part of the object was deposited.
  - In the stress calculations the following issues deserve extra attention:
    * The stress equations as such have no unique solution. They should be coupled to the stress-strain relation of concrete.
    * The boundary condition to be applied at the bottom, so where it is in contact with the table, deserves extra attention. There is friction between object and table, but this friction will depend on the local normal stress.
    * To calculate the stress distribution, it is recommended to make use of standard software based on the Finite Element Method (FEM).

* Analytical approaches also provide useful insights that can be used to check numerical outcomes and for deriving rules of thumb. E.g., for a wall tilted to the right the maximum stress will be attained in the right, lower corner and its value is given by equation (1.68)

Acknowledgements

We kindly acknowledge the contributions of Charlotte Philips and Elise Buiter from Bruil company to accomplish this project. They were very helpful in answering all kind of questions during the modelling week and even organized a guided tour for us through the Bruil facilities. They also critically reviewed earlier drafts of this report and came up with useful suggestions.

Bibliography

[1] N. Umetani, and R. Schmidt, Cross-sectional Structural Analysis for 3D Printing Optimization, in: SIGGRAPH Asia 2013 Technical Briefs, pp. 5:1-5:4, ISBN 978-1-4503-2629-2, http://doi.acm.org/10.1145/2542355.2542361, 2013.

[2] A. Perrot, D. Rangeard, A.F. Pierre, Structural built-up of cement-based materials used for 3D-printing extrusion techniques, Materials and Structures, Vol 49, pp 1213 - 1220, DOI 10.1617/s11527-015-0571-0, 2016.

[3] L. Reiter, T. Wanler,N. Roussel,R.J. Flatt, The role of early age structural build-up in digital fabrication with concrete, Cement and Concrete Research, Vol 112, pp 86 - 95, DOI 10.1016/j.cemconres.2018.05.011, 2018.

[4] N. Roussel, Rheological requirements for printables concretes, Cement and Concrete Research, Vol 112, pp 76 - 85, DOI 10.1016/j.cemconres.2018.04.005, 2018.

[5] A.S.J Suiker, Mechanical performance of wall structures in 3D printing processes: theory. design tools and experiments, International Journal of Mechanical Sciences, Vol 137, pp 145 - 170, DOI 10.1016/j.ijmecsci.2018.01.010, 2018.

[6] Poston, T. and Stewart, I., Catastrophe Theory and Its Applications, Dover Publications, 1996